ARTICLE | Article in Press

Tyrosol ameliorates Urografin induced acute hepatorenal toxicity via Nrf2 and HO1 pathways based on biochemical and histopathological evaluations

Muhammed Etyemez · Tuncer Kutlu

Received: 27 April 2026 / Accepted: 31 August 2026
© The Author(s) 2026

Abstract

The clinical use of iodinated radiocontrast agents (especially Urografin) can lead to contrast-induced nephropathy (CIN) and hepatotoxicity mediated by oxidative stress and inflammation. This study aimed to investigate the protective potential of Tyrosol, a major bioactive component of virgin olive oil, against Urografin-induced acute hepato-renal toxicity. Thirty-two female Wistar albino rats were randomly assigned to four groups ($n=8$). To evaluate the protective efficacy of Tyrosol against contrast-induced toxicity, a 30-day pretreatment model was established. Rats in the treatment cohorts received Tyrosol (20 mg/kg/day) via oral gavage for 30 consecutive days, followed by a single intravenous (IV) injection of Urografin (6 mL/kg) via the tail vein on the 30th day. At 48 h post-injection, serum hepatorenal function markers (urea, creatinine, ALT, AST, ALP, albumin, Ca^{2+}, and inorganic phosphorus) were measured photometrically. Furthermore, liver and kidney tissues were evaluated for oxidative stress indicators (MDA, GSH, GPx, CAT via spectrophotometrically) and pro-inflammatory cytokines (TNF-α, IL-1β, IL-6 via ELISA). For molecular assessments, Nrf-2 and HO-1 protein expressions in kidney tissues were quantified via Western blotting. Finally, liver and kidney sections were stained with hematoxylin and eosin for histopathological evaluation. Urografin administration significantly elevated serum urea, creatinine, and AST levels while decreasing ALP. It induced marked oxidative stress in both liver and kidney tissues by elevating MDA levels and depleting GSH levels and GPx activities, alongside triggering a cytokine storm characterized by increased TNF-α, IL-1β, and IL-6 levels. Tyrosol pretreatment successfully restored serum urea, renal MDA, and hepatic/renal GSH to control levels, and completely normalized TNF-α and IL-1β concentrations. However, the restorations of creatinine, AST, IL-6, and hepatic MDA were partial and did not reach control baseline values. Molecular analyses demonstrated that Urografin suppressed the cellular defense mechanisms, whereas Tyrosol reactivated the Nrf-2/HO-1 signaling pathway by significantly elevating their protein expressions. Histopathologically, Tyrosol significantly ameliorated Urografin-induced hepatic inflammatory infiltration, as well as renal hemorrhage, mononuclear cell infiltration, and hydropic degeneration. Tyrosol (20 mg/kg) provides robust multi-organ protection against Urografin-induced acute hepato-renal injury in a female rat model by intensely reactivating the Nrf-2/HO-1 antioxidant pathway and suppressing the pro-inflammatory cascade.

Keywords Tyrosol · Urografin · Contrast-induced nephropathy · Hepatorenal toxicity · Nrf-2/HO-1

This Article in Press is shared early to give you faster access to new research. It is citable and carries a permanent DOI. The final edited version will replace it automatically.

Published online: 04 September 2026

Introduction

Among the various contrast agents extensively applied in diagnostic imaging and interventional procedures, Urografin is prominent. This iodinated radiographic medium is routinely utilized in both veterinary and human medicine for angiographic applications, including cholangiography and myelography[1,2]. While generally recognized as safe, iodinated agents used in CT scans, intravenous urography, angiography, and indirect radiography can cause serious adverse reactions[3–5]. Notably, Japanese investigators highlighted that the high-osmolar, ionic nature of Urografin presents substantial health hazards, with instances of mortality linked to its inappropriate administration[6]. Due to their minimal plasma protein binding, these agents are typically cleared from healthy individuals within approximately two hours; conversely, this clearance can be prolonged to several weeks in cases of compromised kidney function[7]. Renal excretion accounts for roughly 98% of the administered iodide, with minor routes (lacrimal, sweat, and salivary glands) handling the remaining 2%. Although standard doses do not typically elevate iodide levels enough to trigger sialadenitis, a decline in renal clearance can elevate free iodide concentrations, prompting its accumulation in the salivary glands[8]. Although safer low- and iso-osmolar contrast agents have largely replaced Urografin for direct intravascular imaging in developed countries, it is still routinely utilized for gastrointestinal and body cavity examinations[6]. Furthermore, its cost-effectiveness and high accessibility maintain its prominence in veterinary medicine and developing nations[1,9]. Nevertheless, systemic exposure to this high-osmolar ionic agent carries a significant risk of severe adverse reactions[10–12].

A disruption in the equilibrium between oxidant generation and cellular antioxidant mechanisms, combined with inadequate repair responses, characterizes oxidative stress. Such an imbalance promotes widespread cellular toxicity and subsequent tissue deterioration[13,14]. The administration of contrast media is known to trigger renal artery vasoconstriction, diminishing renal blood perfusion and precipitating ischemia-reperfusion injury[3,15]. An increase in oxidative stress coupled with a decline in nitric oxide bioavailability are central factors driving contrast-induced nephrotoxicity[16,17]. Exposure to Urografin has been shown to elevate malondialdehyde (MDA) levels, a key indicator of oxidative damage, while concurrently suppressing the activity of superoxide dismutase (SOD), a crucial antioxidant enzyme[18]. Moreover, this ionic medium triggers apoptotic pathways in renal tubular cells by modulating signals associated with endoplasmic reticulum (ER) stress, where Caspase-12 activation plays a mediating role[12]. Urografin also provokes inflammatory responses that culminate in functional nephropathy and structural alterations. Corresponding histopathological assessments show structural anomalies such as mononuclear cell infiltration, vascular congestion, tubular cell vacuolization, and widened proximal and distal convoluted tubules[9,11].

Conversely, the application of tyrosol substantially bolsters renal antioxidant networks and diminishes MDA accumulation, thereby safeguarding both kidney function and its histological integrity[19–21]. Notably, tyrosol demonstrates superior efficacy in these protective roles compared to whole olive oil[22,23]. Tyrosol (2-[4-hydroxyphenyl]ethanol) is a naturally occurring antioxidant widely distributed in the leaves and fruits of the olive plant (Oleaceae family)[24]. The phenolic hydroxyl group within its structure plays a pivotal role in mediating both its antioxidant and antimicrobial activities[25]. Tyrosol has been reported to exhibit a broad spectrum of biological properties, exerting antioxidant, anti-apoptotic, and anti-inflammatory effects across various target organs[26]. Recent studies have demonstrated that it manifests anticancer properties via the inhibition of the NF-κB/HIF-1α signaling pathway, whereas its antioxidative effects are driven by the activation of the Nrf-2/HO-1 pathway[27,28]. Furthermore, it exerts robust anti-inflammatory efficacy by suppressing LOX-5 and MPO activities[29]. By suppressing oxidative stress and inflammation, tyrosol exhibits strong nephroprotective properties against acute kidney injury[30]. Tyrosol can be utilized as an anti-inflammatory agent either standalone or in combination with other commercially available drugs; notably, it presents minimal adverse effects and contraindications compared to current state-of-the-art prescription NSAIDs[31].

Despite the known toxicities associated with high-osmolar contrast media like Urografin, effective and safe prophylactic strategies to prevent subsequent hepato-renal damage remain a significant challenge in clinical

practice[9,16,32]. Furthermore, while the general antioxidant potential of tyrosol has been reported in various injury models, a distinct gap remains in the literature: its specific therapeutic efficacy and underlying molecular mechanisms-particularly concerning the Nrf-2/HO-1 pathway-against Urografin-induced multi-organ toxicity have not been previously investigated. Addressing this critical research gap, the present study seeks to explore how tyrosol mitigates oxidative injury and hepato-renal inflammation triggered by Urografin exposure. Accordingly, the present study seeks to explore how tyrosol mitigates oxidative injury and hepato-renal inflammation triggered by Urografin exposure. To achieve this, hepatic and renal functions were monitored using panels of urea, creatinine, ALT, AST, ALP, albumin, Ca^{2+}, and inorganic phosphorus (P). The tissue redox state was evaluated through MDA, GSH, GPx, and CAT assays. Furthermore, the investigation encompassed the assessment of pro-inflammatory cytokines (IL-6, TNF-α, and IL-1β), the analysis of Nrf-2/HO-1 signaling cascades, and tissue histopathology.

Materials and methods

Ethical statement

The Kastamonu University Local Animal Ethics Committee approved all animal handling and experimental protocols prior to the commencement of the study (Approval Date: March 17, 2025; Issue: 5, Decision No: 15; Protocol No: E-16498365-050.04-2500038477). Every procedure strictly adhered to the guidelines outlined in the "Guide for the Care and Use of Laboratory Animals." Furthermore, to minimize experimental variance, all analytical measurements were performed in triplicate. The study was conducted in accordance with the Basic and Clinical Pharmacology and Toxicology policy for experimental and clinical studies[33].

Chemicals and reagents

The high-osmolar ionic contrast agent employed in this study was Urografin (76%, 50 mL, meglumine/sodium diatrizoate), supplied by Bayer, Germany. Sigma-Aldrich Chemical Company provided the Tyrosol. Cytokine quantification kits (IL-6, TNF-α, and IL-1β ELISA) were sourced from Bioassay Technology Laboratory (Shanghai Korain Biotech Co., Ltd.). Additionally, Proteintech Group, Inc. supplied all primary antibodies (Nrf-2, NF-κB, beta-actin) alongside the corresponding HRP-linked secondary antibodies.

Animals

Thirty-two female Wistar albino rats (body weight range: 180–250 g) were procured from the Karabük University Experimental Animal Center. The subjects were randomly assigned to four equal cohorts ($n=8$ per group) and housed at the Kastamonu University Experimental Animal Research and Application Center. Housing environments were tightly regulated, maintaining a temperature of 21 ± 1 °C under a 12-h light/12-h dark cycle. Access to standard pelleted chow and tap water was provided *ad libitum* throughout the duration of the study.

Experimental design

- Control Group: Rats were administered 1 mL of physiological saline via oral gavage every day for 30 consecutive days. On the 30th day, they received a single 6 mL/kg intravenous (IV) injection of physiological saline through the tail vein.

- Urografin Group: Similar to the control cohort, these rats received daily oral physiological saline (1 mL) for 30 days. On the final day, contrast toxicity was induced using a single IV tail vein injection of Urografin at a dosage of 6 mL/kg[11].
- Tyrosol (Tyr) Group: Animals in this cohort received an oral gavage of Tyrosol (20 mg/kg dissolved in 1 mL saline) daily for 30 days[34]. This was followed by a single IV saline injection (6 mL/kg) via the tail vein on the final day.
- Urografin + Tyrosol (Uro + Tyr) Group: This group underwent a 30-day oral pretreatment with Tyrosol (20 mg/kg in 1 mL saline). On the 30th day, a single 6 mL/kg IV dose of Urografin was injected into the tail vein.

At 48 h post-IV injection, all subjects were anesthetized using an intramuscular combination of ketamine (60 mg/kg) and xylazine (10 mg/kg). Under deep anesthesia, blood was drawn via cardiac puncture, and the resulting serum was separated for functional testing. Following blood collection, the animals were euthanized by decapitation. Immediately thereafter, the liver and kidney tissues were rapidly excised, washed in physiological saline, and flash-frozen at −80 °C pending downstream biochemical evaluations.

Hepatorenal function tests

Measurements of urea, creatinine, ALT, AST, ALP, albumin, Ca^{2+}, and inorganic phosphorus (P) in the serum samples were performed photometrically using a Beckman Coulter AU 5800 clinical chemistry autoanalyzer (Beckman Coulter Inc., CA, USA) and the manufacturer's proprietary reagents.

Biochemical analyses of oxidative stress

Kidney and liver tissues, previously stored at −80 °C, were transferred to glass tubes and maintained on ice to preserve enzymatic integrity. Once excised, the tissues were homogenized to assess their antioxidant capacity and lipid peroxidation levels. The tissues were homogenized in a cold 1.15% potassium chloride (KCl) buffer (1:10, w/v). To ensure precise normalization of all subsequent calculations, the total protein concentration within these homogenates was quantified using a Bicinchoninic Acid (BCA) Protein Assay Kit. Following protein determination, the homogenates were centrifuged at 5000 × g for 1 h at +4 °C, and the resulting supernatants were carefully separated for downstream spectrophotometric assays.

To gauge lipid peroxidation, the concentration of thiobarbituric acid reactive substances was analyzed. Specifically, malondialdehyde (MDA) a primary aldehyde product of lipid peroxidation, forms a pink-colored complex upon reaction with thiobarbituric acid. The degree of lipid peroxidation was determined by measuring the absorbance of this complex at 532 nm, and the results were reported as nmol/g of total protein[35]. Glutathione (GSH) content was evaluated following the protocol established by Sedlak and Lindsay[36]. This method utilizes 5,5'-dithio-bis(2-nitrobenzoic acid) (DTNB), which is reduced by sulfhydryl compounds to yield a highly yellow anion. The color intensity of the resulting complex, which is directly proportional to the GSH concentration, was measured spectrophotometrically at 412 nm and presented as nmol/g protein. For glutathione peroxidase (GPx, EC 1.11.1.9) activity, the assay detailed by Lawrence and Burk[37] was employed. This procedure relies on the GPx-catalyzed oxidation of GSH to oxidized glutathione (GSSG) via a peroxide substrate. Subsequently, GSSG is reduced back to GSH by glutathione reductase with the concomitant oxidation of NADPH to $NADP^+$. The enzyme activity was determined by continuously monitoring the decrease in absorbance at 340 nm, yielding results in international units (IU) per gram of protein. Finally, catalase (CAT, EC 1.11.1.6) activity was assessed by tracking the breakdown of hydrogen peroxide (H_2O_2)[38]. The enzymatic decomposition rate of H_2O_2 was measured spectrophotometrically at 240 nm by recording the absorbance difference over a 30-second interval. CAT activity was calculated and expressed as the rate constant (k) per gram of protein.

Measurement of TNF-α, IL-1β, and IL-6 inflammation markers

Prior to the analyses, the tissues were homogenized in PBS. Subsequently, the samples were centrifuged, and the resulting supernatants were transferred into microtubes. The levels of TNF-α (E0764Ra; BT LAB), IL-1β (E0119Ra; BT LAB), and IL-6 (E0135Ra; BT LAB) were measured in 96-well plates using the enzyme-linked immunosorbent assay (ELISA) method. The measurements were performed at 450 nm using an ELISA reader (EPOCH Take3Plate, BioTek) in accordance with the manufacturer's protocol.

Western blot analysis of Nrf-2/HO-1 markers

Upon completion of the experiment, harvested kidney tissues were homogenized in RIPA lysis buffer (sc-24948/SantaCruz) supplemented with a protease inhibitor cocktail. The total protein content of the lysates was quantified using a BCA Protein Assay Kit (Thermo Scientific). Prior to electrophoresis, the protein extracts were mixed with a sample buffer and denatured at 95 °C for 10 min. Aliquots containing 20 µg of protein were resolved on a 10% SDS-polyacrylamide gel at 150 V for 60 min[39]. Following electrophoretic separation, the proteins were electroblotted onto PVDF membranes. To minimize non-specific binding, these membranes were blocked in 5% dry milk for one hour at room temperature. They were then probed overnight at 4 °C with primary antibodies specific for Nrf-2 (Proteintech, Rosemont, IL, USA; Cat No:16396-1-AP) and HO-1 (Proteintech, Rosemont, IL, USA; Cat No:10701-1-AP). After a 15-minute wash with Tris buffer, the blots were incubated for another hour at room temperature with HRP-conjugated secondary antibodies (Abcam, Cambridge, United Kingdom; Cat No: ab6734). Post-incubation, the membranes underwent three consecutive 5-minute washes with PBS-T. Immunoreactive bands were visualized using an ECL substrate (Clarity Western ECL Substrate, BioRad, 1705060) on a GE LAS 500 imaging system (GE Healthcare Bio-Sciences AB). Finally, densitometric quantification of the bands was performed using ImageJ software (v1.54, NIH, USA), where target protein intensities were normalized against β-actin (Proteintech, Rosemont, IL, USA; Cat No:20536-1-AP), the endogenous control, and reported as arbitrary units[40].

Histopathological procedures

Following euthanasia, a necropsy was performed on all animals. Liver and kidney tissues were excised and fixed in 10% buffered formalin. Following routine processing through graded alcohol and xylene series, the tissues were embedded in paraffin. Sections of 5 µm thickness were obtained, deparaffinized in xylene, rehydrated through a descending alcohol series (100%, 96%, 80%, and 70%), and stained with Hematoxylin and Eosin (H&E). Histopathological evaluation of the stained sections was performed under a light microscope (Olympus CX31) by a pathologist in a blinded manner regarding group assignments, and microphotographs were captured (Olympus DP12). Histopathological findings in the liver and kidney were evaluated according to the following grading criteria: Grade 0: Histopathological changes affecting less than 5% of the area; Grade 1: Mild histopathological changes involving between 5% and 33% of the total area; Grade 2: Moderate histopathological changes involving between 33% and 66% of the total area; Grade 3: Severe histopathological changes involving more than 66% of the total area[41,42].

Statistical analysis

Statistical analyses were performed using IBM SPSS Statistics 23.0 software. Prior to the main analyses, the assumption of normality was evaluated using the Shapiro-Wilk test, and the homogeneity of variances was confirmed via Levene's test. For normally distributed data, comparisons among groups were conducted using one-way analysis of variance (ANOVA) followed by Tukey's post hoc test. Furthermore, to account for multiple comparisons across various biochemical and inflammatory parameters, p-values were adjusted using the

Benjamini-Hochberg False Discovery Rate (FDR) method. Results are presented as mean ± standard deviation (SD) graphs using GraphPad Prism 8.0.2, and p-value ≤ 0.05 is considered statistically significant.

Results

Biochemical findings

The Urografin group significantly increased urea levels compared to the control group ($p < 0.05$), and this parameter decreased to control levels in the Uro + Tyr group. Similarly, creatinine levels were higher in the Urografin group ($p < 0.01$) and were observed not to decrease to normal values in the Uro + Tyr group. Urografin significantly increased AST values compared to the control ($p < 0.001$); however, tyrosol administration failed to restore this enzyme level to control levels. ALP enzyme levels significantly decreased in the Urografin group ($p < 0.05$) and remained at the same level in the Uro + Tyr group. No significant differences were found in ALT, albumin, Ca, and P levels (Fig. 1).

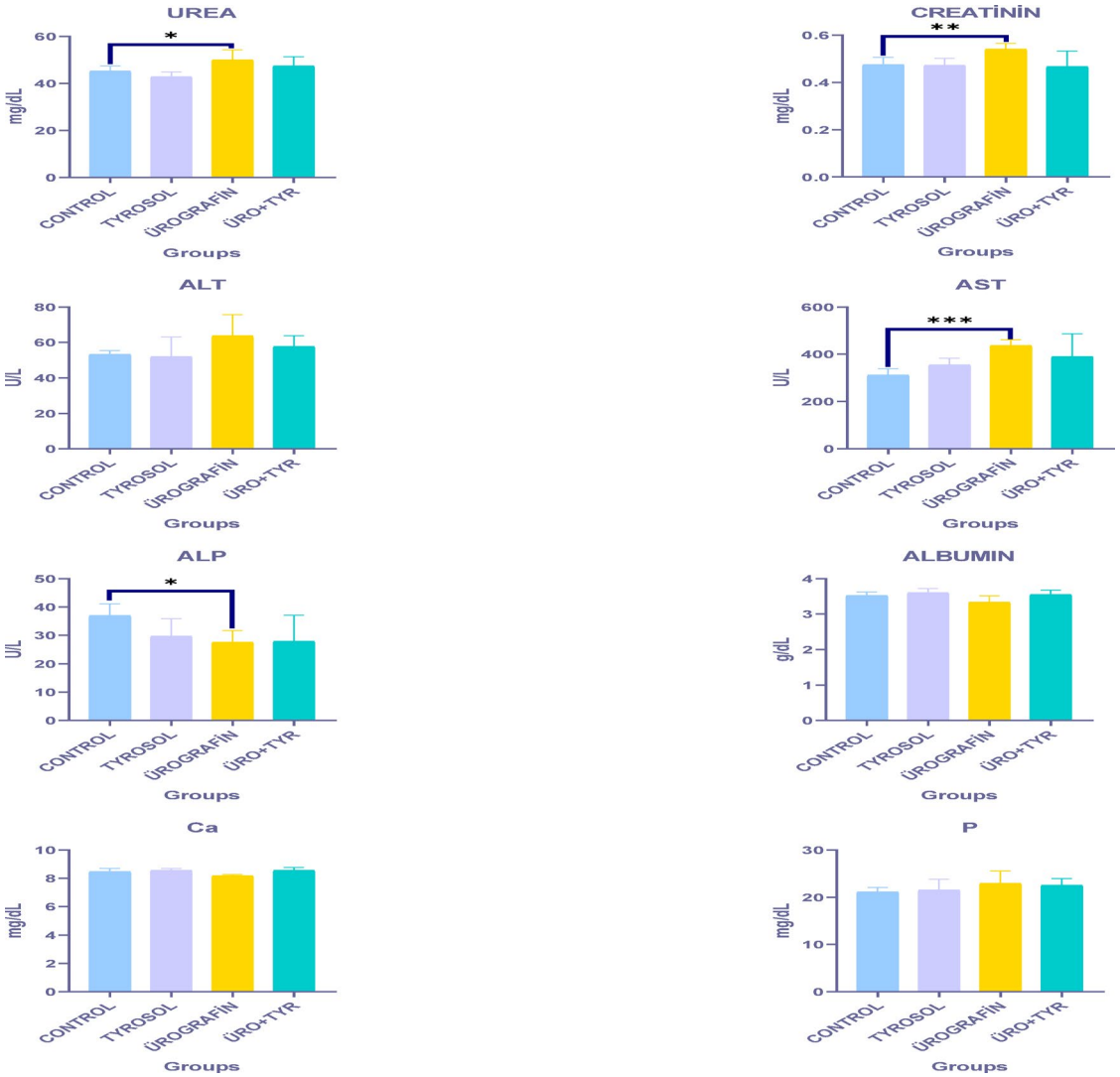


Fig. 1 Hepatorenal serum functional tests, by GraphPad Prism 8.0.2 (*$p < 0.05$, **$p < 0.01$, ***$p < 0.001$).

Oxidative stress in liver and kidney

In the liver, Urografin increased MDA levels compared to the control ($p<0.001$); although it significantly decreased with tyrosol administration in the Uro+Tyr group but it didn't reach the control level. Hepatic GSH levels significantly decreased in the Urografin group compared to the control ($p<0.001$). The Uro+Tyr group, however, restored this enzyme activity to normal levels. No significant differences were determined in hepatic GPx and CAT enzyme activities (Fig. 2).

In kidney tissue, MDA levels were significantly higher in the Urografin group than in the control group ($p<0.05$). The group supplemented with tyrosol reduced these levels back to the control level. GSH levels significantly decreased in the Urografin group ($p<0.001$). In the Uro+Tyr group, this value exceeded the control levels. The Urografin group significantly decreased GPx activity ($p<0.05$). However, in the group treated with tyrosol (Uro+Tyr), this enzyme activity did not reach control levels. No significant differences were observed among the groups in CAT activity (Fig. 2).

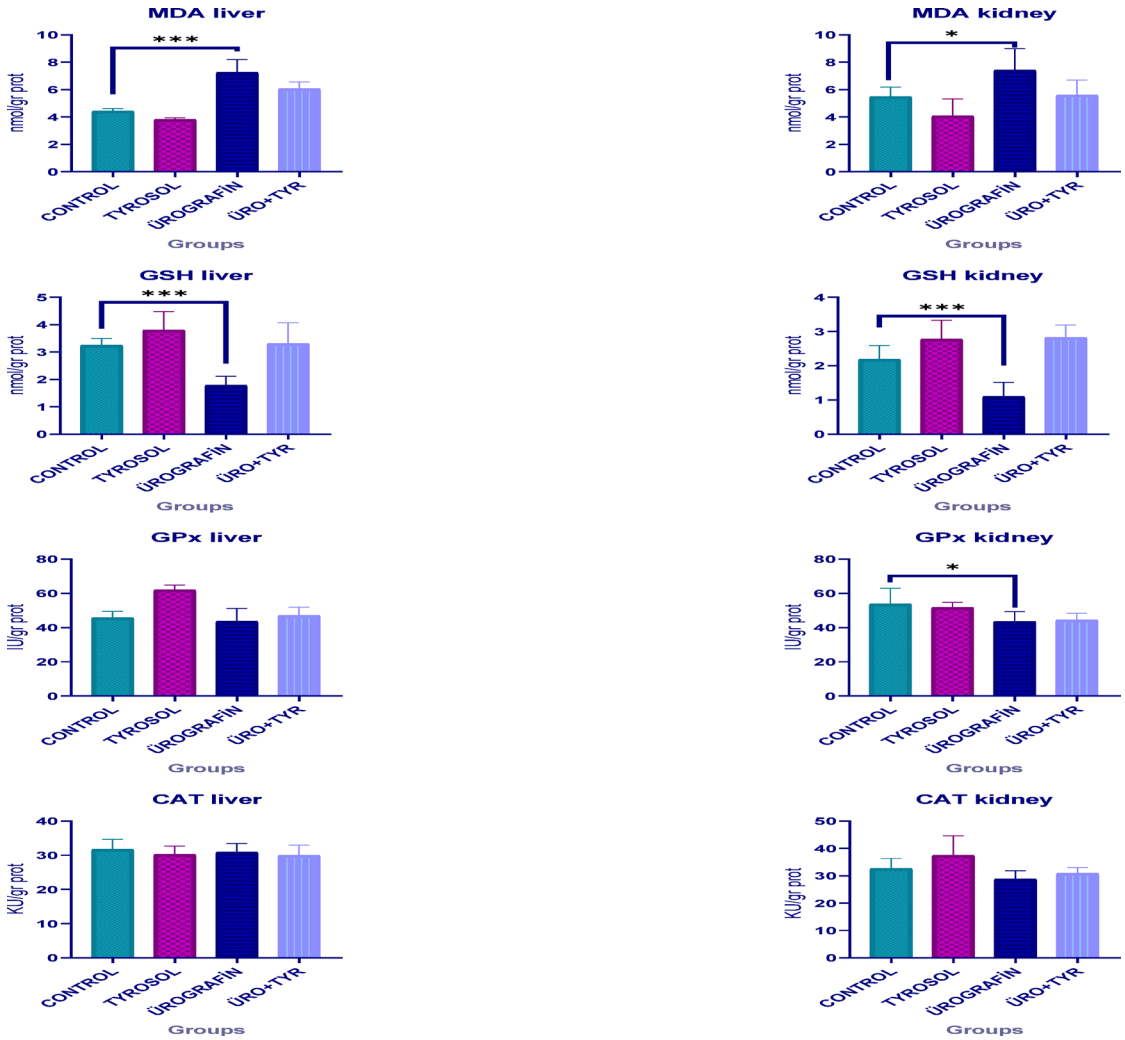


Fig. 2 Oxidant-antioxidant biochemical analyses (*$p<0.05$, **$p<0.01$, ***$p<0.001$).

Cytokine levels

Urografin caused a cytokine storm by significantly increasing the cytokines IL-1β, IL-6, and TNF-α ($p<0.001$). IL-1β and TNF-α cytokine levels decreased to control levels in the Uro+Tyr group. However, IL-6 levels did not decrease to control levels in the Uro+Tyr group (Fig. 3).

Western blotting results

In Western blotting of kidney tissue, the tyrosol group showed significantly higher Nrf-2/HO-1 levels than the control group ($p<0.001$). Furthermore, the Urografin group reduced the Nrf-2 level even below the control ($p<0.01$). The Uro+Tyr group restored these values to the control level and even succeeded in elevating the HO-1 level above the control (Fig. 4).

Histopathological findings

The liver exhibited a normal histological appearance in the control and tyrosol groups (Fig. 5a, b). In the Urografin group, hyperemia in the liver, mild steatosis in hepatocytes, and inflammatory cell infiltration, particularly in the portal tract, were observed (Fig. 5c). In the treatment group, it was noted that tyrosol only reduced inflammatory cell infiltration in a statistically significant manner (Fig. 5d). Although it reduced hyperemia and steatosis, these reductions were not statistically significant (Table 1).

The kidney also exhibited a normal histological appearance in the control and tyrosol groups (Fig. 6a and b). In the Urografin group, however, mild hyperemia, hemorrhage, inflammatory cell infiltration, and hydropic degeneration in the tubular epithelium were present in the kidneys (Fig. 6c–e). In the treatment group, it was observed that hemorrhage, mononuclear cell infiltration, and hydropic degeneration decreased to a statistically significant degree (Fig. 6f; Table 2).

Discussion

The clinical use of iodinated radiocontrast agents (RCAs), particularly ionic and high-osmolar agents such as Urografin, disrupts cellular membrane integrity and induces intrarenal vasoconstriction, thereby leading to contrast-induced nephropathy (CIN) and secondary hepatotoxicity[5,32,43,44]. Indeed, a recent study by Okonkwo et

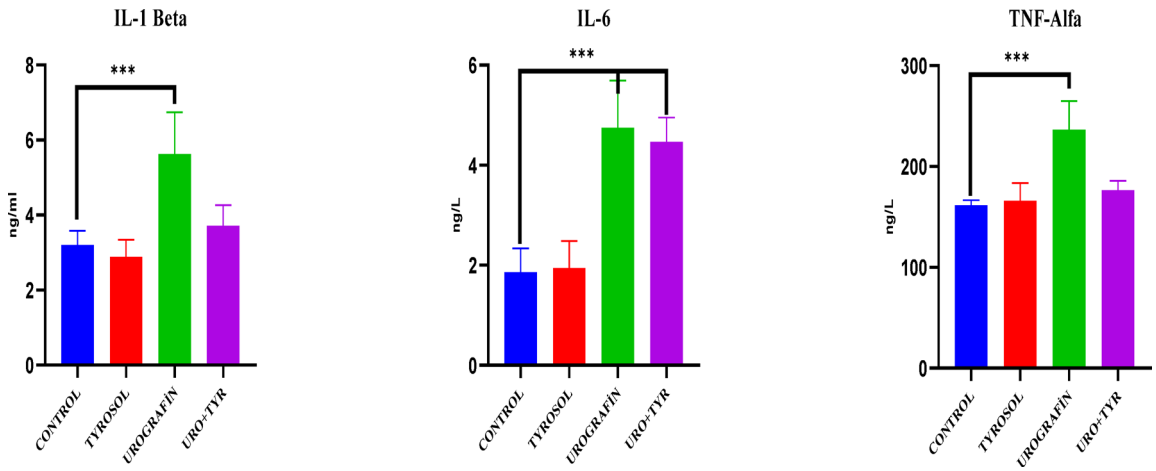


Fig. 3 Analyses of IL-1β, IL-6, and TNF-α cytokines (*$p<0.05$, **$p<0.01$, ***$p<0.001$).

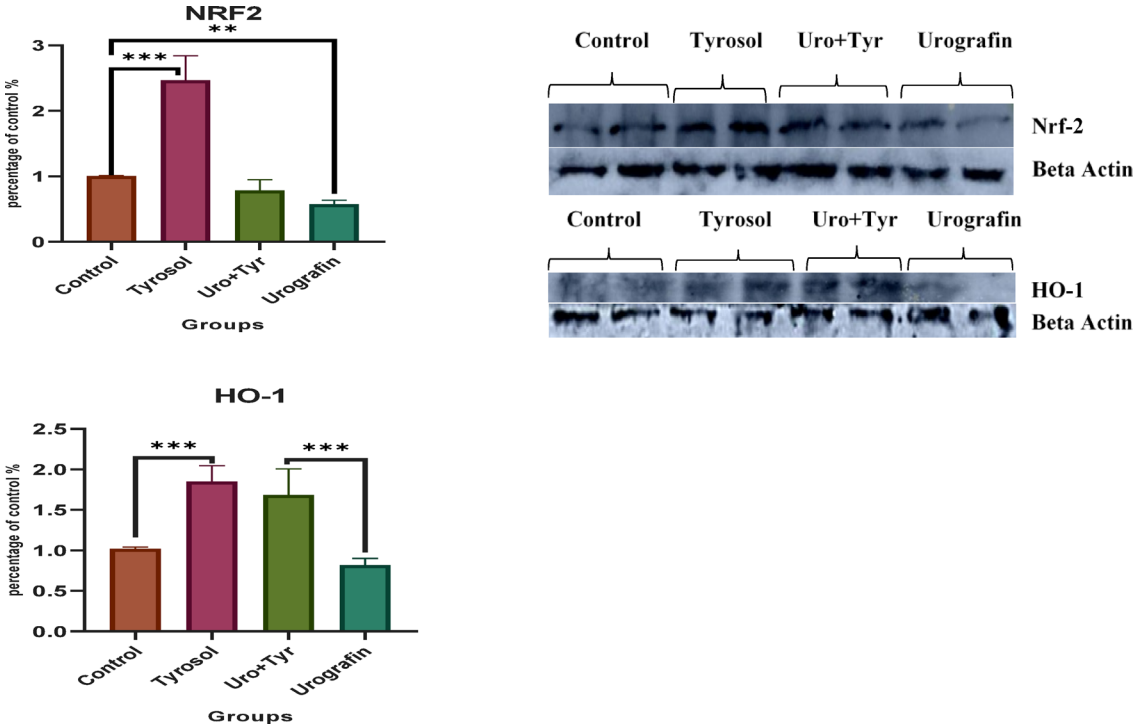


Fig. 4 Western blot analysis of Nrf-2/HO-1. Cropped stain images from the original membrane stains are expressed according to groups. In the graphs, percentages are calculated relative to the control. (*$p<0.05$, **$p<0.01$, ***$p<0.001$).

al.[9] confirmed that exposure to ionic contrast agents specifically impairs hepato-renal functions and dramatically elevates systemic toxicity markers. In our study, the increase in serum urea, creatinine, and AST levels in the Urografin-administered group indicates a decline in renal filtration capacity and hepatocyte membrane damage. In the treatment group, the restoration of these biochemical parameters to control values by Tyrosol one of the major phenolic compounds in extra virgin olive oil indicates the potent efficacy of this bioactive molecule in preventing cellular shock and preserving organ functions.

The most destructive factor of radiocontrast toxicity at the cellular level is the severe oxidative stress caused by reactive oxygen species (ROS)[4]. Hassem[11] reported that intravenous contrast media administration immediately triggers systemic oxidative stress in rats. In our findings, while Urografin increased MDA a degradation product of the cell membrane in the liver and kidney, it completely depleted the reserves of GSH and GPx, which serve as the cellular defense shield. A study at the light and electron microscopic level by Amer and Elabd[10] clearly demonstrated that synthetic antioxidants such as N-acetylcysteine (NAC) provide cellular protection against Urografin-induced renal tubular damage. In our study, Tyrosol administration, similar to synthetic agents, substantially reversed oxidative stress in the kidney and liver through its robust antioxidant capacity.

However, it is noteworthy that Tyrosol didn't completely reduce MDA levels to the control baseline in the liver and didn't fully restore GPx values in the kidney. Because the liver is the primary detoxification center, its subjection to high metabolic stress under an acute toxic load may have delayed the repair process. As demonstrated by Okonkwo et al.[9], in their hepato-renal oxidative stress models, the complete restoration of primary enzymatic activity (such as GPx) requires more time than the replenishment of the cellular GSH pool.

Oxidative stress triggers the pro-inflammatory cascade by activating the NF-κB pathway in tissues[45]. The elevated levels of TNF-α, IL-1β, and IL-6 in the Urografin group indicate a necrotizing, systemic inflammatory response. Tyrosol treatment markedly suppressed inflammatory mediators (particularly TNF-α and IL-1β) by antagonizing the TLR4/NF-κB signaling pathway[46]. The inability of Tyrosol to completely normalize IL-6 can

https://doi.org/10.1038/s41598-026-69817-4

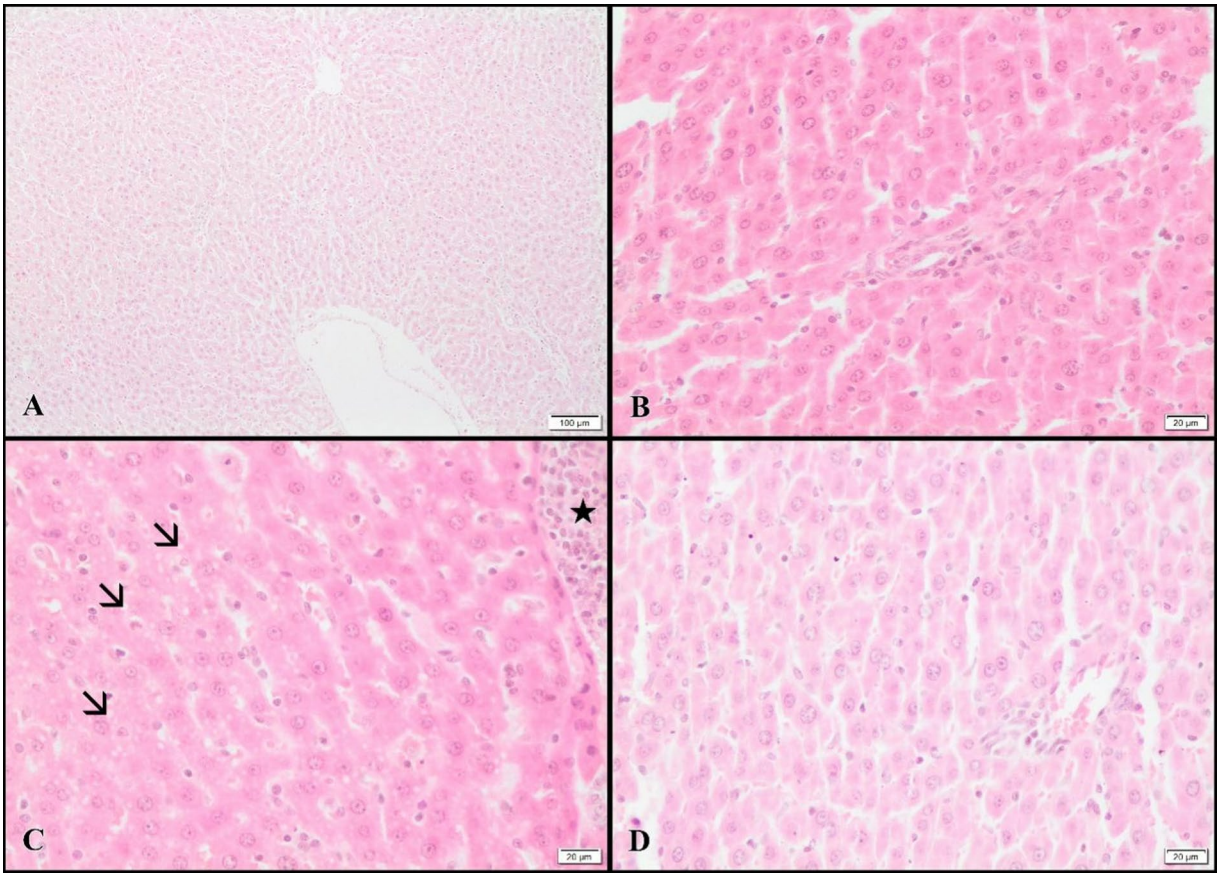


Fig. 5 Histopathological findings in the liver, H&E staining. (**a)** Normal histological structure of the liver, Control group. (**b)** Normal histological structure of the liver, Tyrosol group. (**c)** Lipid vacuoles in hepatocytes (arrows) and inflammatory cell infiltration (asterisk) in the liver, Urografin group. (**d)** Normal histological structure of the liver, Treatment group.

Table 1 Scoring statistics of histopathological findings observed in the liver.

Parameters	Group	Mean	Standard deviation	*P* value
Hyperemia	Control	0.2500	0.46291	<0.142
	Urografin	0.7500	0.46291	
	Tyrosol	0.3750	0.51755	
	Uro+Tyr	0.2500	0.46291	
Liposis	Control	0.0000[a]	0.00000	<0.096
	Urografin	0.5000[b]	0.03452	
	Tyrosol	0.1250[ab]	0.15355	
	Uro+Tyr	0.2500[ab]	0.06291	
Inflammatory cell infiltration	Control	0.0000[a]	0.00000	<0.001***
	Urografin	0.8750[b]	0.35355	
	Tyrosol	0.0000[a]	0.00000	
	Uro+Tyr	0.2500[a]	0.12598	

[a, b,c]Different letters in the rows in the "Mean" column indicate statistical significance between groups. ($P<0.05$).

be explained by the fact that this cytokine is a pleiotropic molecule also involved in tissue repair processes (e.g., hepatocyte regeneration)[47].

The molecular findings of our study place the multi-organ protective Nrf-2/HO-1 pathway[48] at the center of Tyrosol's cellular protection mechanism. While the suppression of Nrf-2 by Urografin paralyzes the cellular defense, Tyrosol's profound upregulation of Nrf-2 and HO-1 expression recharged the endogenous defense

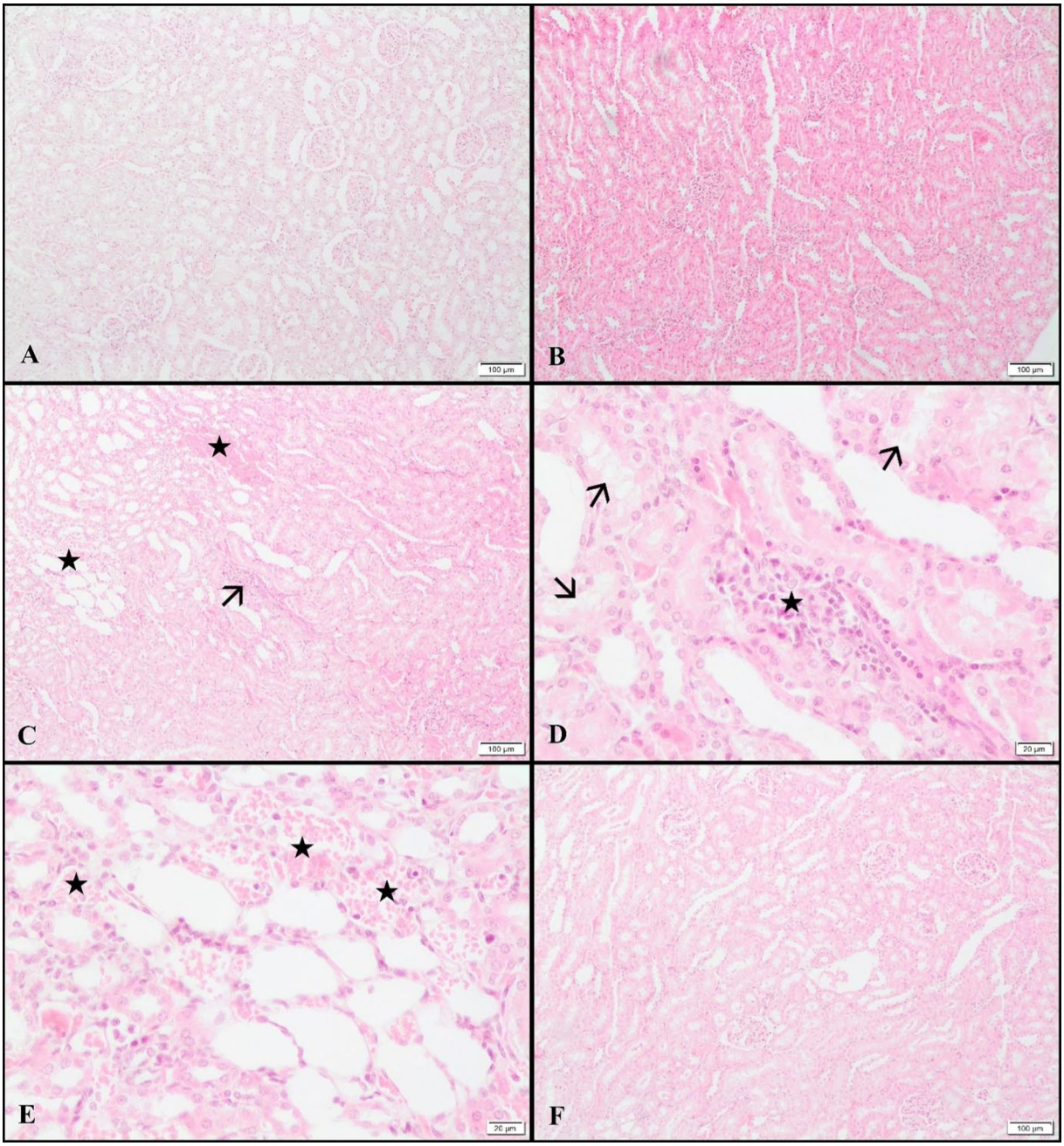


Fig. 6 Histopathological findings in the kidneys, H&E staining. (**a)** Normal histological structure of the kidney, Control group. (**b)** Normal histological structure of the kidney, Tyrosol group. (**c)** Hemorrhage (asterisks) and inflammatory cell infiltration (arrow) in the kidneys, Urografin group. (**d)** Hydropic degeneration in the tubular epithelium (arrows) and inflammatory cell infiltration (asterisk) in the kidneys, Urografin group. (**e)** Hemorrhage (asterisks) in the kidneys, Urografin group. (**f)** Normal histological structure of the kidney, Treatment group.

system. It has been clearly demonstrated in the literature that, in acute organ injury models, endogenous antioxidant defense can be restored only when the Nrf-2/HO-1 system is triggered by a potent inducer[49].

Our biochemical and molecular findings are in perfect alignment with the histopathological tissue analyses demonstrating the microvascular endothelial dysfunction caused by Urografin. Emad et al.[50], and Hassem et al.[11], extensively reported that Urografin administration leads to severe degeneration, hemorrhage, and ultrastructural destruction in rat renal tubules[11,50]. It is known that pharmacological agents such as nebivolol[50,51],

Table 2 Scoring statistics of histopathological findings observed in the kidney.

Parameters	Group	Mean	Standard deviation	*P* value
Hyperemia	Control	0.2500	0.46291	<0.142
	Urografin	0.7500	0.46291	
	Tyrosol	0.3750	0.51755	
	Uro+Tyr	0.2500	0.46291	
Hemorrhage	Control	0.0000[a]	0.00000	<0.001***
	Urografin	0.8750[b]	0.83452	
	Tyrosol	0.0000[a]	0.00000	
	Uro+Tyr	0.1250[a]	0.35355	
Hydropic degeneration	Control	0.0000	0.00000	<0.096
	Urografin	0.5000	0.53452	
	Tyrosol	0.1250	0.35355	
	Uro+Tyr	0.2500	0.46291	
Inflammatory cell infiltration	Control	0.0000[a]	0.00000	<0.001***
	Urografin	0.8750[b]	0.35355	
	Tyrosol	0.0000[a]	0.00000	
	Uro+Tyr	0.2500[a]	0.46291	

[a, b,c]Different letters in the rows in the "Mean" column indicate statistical significance between groups ($P<0.05$).

atorvastatin[11] and tadalafil[52] provide histological protection in preventing contrast-induced nephropathy. In our study, the statistically significant amelioration of structural degeneration in the kidney (hemorrhage, mononuclear cell infiltration, and hydropic degeneration) by Tyrosol, a natural compound, proves that it exhibits a potent nephroprotective profile comparable to synthetic agents. The lack of complete recovery in hepatic hyperemia and steatosis indicates that the repair process of the histological tissue architecture is still ongoing.

Conclusion

In conclusion, the present study indicates that Urografin can induce contrast-induced nephropathy and secondary hepatotoxicity by triggering an oxidative stress cascade and compromising cellular antioxidant defenses. Tyrosol intervention demonstrated a protective potential against this multi-organ toxicity. Specifically, it contributed to the improvement of key kidney function markers by reducing peak urea levels (from approximately 60 mg/dL in the Urografin group to ~45 mg/dL in the treatment group), attenuated the elevation of pro-inflammatory cytokines by reducing peak TNF-α (from ~250 pg/mL to ~140 pg/mL) and IL-1β (from ~85 pg/mL to ~45 pg/mL), and mitigated tissue hemorrhage in the renal tubules. Furthermore, our findings suggest that Tyrosol's protective effects may be mediated through the upregulation of the Nrf-2/HO-1 pathway, restoring Nrf-2 expression from approximately 60% up to control levels (~100%) and elevating HO-1 levels to ~120%. While further studies with optimized dosages or longer durations are necessary to fully elucidate its effect on hepatic oxidative damage, Tyrosol shows promise as a supportive natural adjuvant to help alleviate radiocontrast-associated morbidity. Future clinical trials will be essential to evaluate its therapeutic applicability.

Limitations

Although our findings provide robust evidence for the protective effects of Tyrosol against Urografin-induced hepato-renal toxicity, our study has certain methodological and translational limitations:

- Animal Model and Clinical Translation: This study was conducted using an in vivo Wistar rat model. Although the renal physiology and hepatic metabolism of rats exhibit significant similarities to those of humans, the pharmacokinetics of radiocontrast agents and the exact clinical picture of Contrast-Induced Nephropathy

(CIN) pathogenesis in humans may not fully align with animal models. Therefore, further reproducibility data are required for the direct extrapolation of these findings to human clinical trials.

- Lack of a Dose-Response Relationship: In this study, Urografin and Tyrosol (20 mg/kg) were administered following a specific, fixed regimen. The inability of the 20 mg/kg Tyrosol dose to fully restore hepatic MDA levels and renal GPx activities to baseline control levels suggests that the "optimal protective dose" for these parameters might be higher. Future studies establishing a reproducible dose-response curve involving varying dosages of Tyrosol (e.g., 10, 20, and 40 mg/kg) will more clearly define the therapeutic window.
- Acute Phase Evaluation: The present study focused on the "acute" effects of contrast agent toxicity and short-term cellular repair. The incomplete normalization of IL-6 levels and the failure to fully restore the histopathological architecture of the liver (hyperemia and steatosis) indicate that tissue repair processes are still ongoing. Longer observation periods (e.g., 14 or 28 days) are necessary to elucidate the long-term tissue regenerative capacity of the molecule in the chronic phase.
- Lack of Molecular Cross-talk Evaluation: Although the protective effect of Tyrosol was predominantly elucidated via Nrf-2/HO-1 activation, the apoptosis cascade (Caspase-3, Bax/Bcl-2 ratio) and cell survival pathways (PI3K/Akt or MAPK) were not comprehensively investigated through specific protein expression analyses in this study.
- Some New Advanced Biomarkers: While classical markers (urea and creatinine) combined with oxidative stress parameters successfully demonstrated Urografin-induced nephrotoxicity in our model, future studies should consider incorporating highly precise early biomarkers, such as Cystatin C and KIM-1, to further detail the temporal dynamics of tubular injury.

Supplementary Information The online version contains supplementary material available at https://doi.org/10.1038/s41598-026-69817-4.

Author contributions M.E. conceptualized the study, designed the experimental protocol, and supervised the overall project. M.E. and T.K. conducted the in vivo animal experiments and collected the tissue samples. M.E. performed the biochemical assays and Western blot analyses. T.K. carried out the histopathological examinations and scoring. M.E. analyzed the data, performed the statistical analyses, and generated the figures. M.E. drafted the original manuscript. All authors actively participated in reviewing and editing the manuscript. All authors have read and approved the final version of the manuscript.

Data availability The datasets generated and/or analysed during the current study are available from the corresponding author on reasonable request.

Declarations

Competing interests The authors declare no competing interests.

Open Access This article is licensed under a Creative Commons Attribution-NonCommercial-NoDerivatives 4.0 International License, which permits any non-commercial use, sharing, distribution and reproduction in any medium or format, as long as you give appropriate credit to the original author(s) and the source, provide a link to the Creative Commons licence, and indicate if you modified the licensed material. You do not have permission under this licence to share adapted material derived from this article or parts of it. The images or other third party material in this article are included in the article's Creative Commons licence, unless indicated otherwise in a credit line to the material. If material is not included in the article's Creative Commons licence and your intended use is not permitted by statutory regulation or exceeds the permitted use, you will need to obtain permission directly from the copyright holder. To view a copy of this licence, visit http://creativecommons.org/licenses/by-nc-nd/4.0/.

References

1. Kalang, J. J., Bata, S. I., Malam, P. A., Tanko, P. N. & Jamparda, J. Evaluation of dexamethasone and methylprednisolone administration on visceral organs prior to contrast radiography in Nigerian indigenous breed of dogs (2022).

2. Shimada, R., Ezaki, J. & Kibayashi, K. Dose-dependent mortality involving convulsions due to subarachnoid Urografin® injection in rats. *Leg. Med.* **29**, 29–33 (2017).
3. Cho, E. & Ko, G. J. The pathophysiology and the management of radiocontrast-induced nephropathy. *Diagnostics* **12** (1), 180. https://doi.org/10.3390/diagnostics12010180 (2022).
4. McCullough, P. A. Contrast-induced acute kidney injury. *J. Am. Coll. Cardiol.* **51** (15), 1419–1428. https://doi.org/10.1016/j.jacc.2007.12.035 (2008).
5. Wong, P. C., Li, Z., Guo, J. & Zhang, A. Pathophysiology of contrast-induced nephropathy. *Int. J. Cardiol.* **158**(2), 186–192. https://doi.org/10.1016/j.ijcard.2011.06.115 (2012).
6. Okuyama, E. et al. Radiologist expertise and responsibilities for off-label use of Urografin before the change in indication by medical health insurance. *Jpn. J. Radiol.* **41**, 909–910. https://doi.org/10.1007/s11604-023-01404-3 (2023).
7. Aydin Çelik, Ö., Aydin, S. & Güney, H. Z. *Ankara Eğt Arş Hast Derg* **53** (1), 61–67 (2020).
8. Nazzaro, P. et al. Iodide mumps following low-osmolarity contrast medium use in haemodialysis patients. *G Ital. Nefrol.* **30** (1), 7 (2013).
9. Okonkwo, A. et al. Assessment of hepato-renal functions and markers of oxidative stress in animals exposed to ionic contrast media. *Jordan J. Biol. Sci.* **17** (3), 1 (2024).
10. Amer, R. M. & Elabd, S. S. Deleterious effect of urografin on the renal tubules of adult albino rats and the possible protective effect of N-acetylcysteine light and electron microscopic study. *Egypt. J. Histol.* **42** (3), 730–739. https://doi.org/10.21608/ejh.2019.11244.1105 (2019).
11. Hassem, A. et al. Atorvastatin ameliorates Urografin induced nephropathy in the presence of dehydration as a risk factor: a histological and morphometric study on a rat model. *Egypt. J. Anat.* **43** (2), 250–274. https://doi.org/10.21608/eja.2024.269411.1124 (2024).
12. Wu, C. T., Weng, T. I., Chen, L. P., Chiang, C. K. & Liu, S. H. Involvement of caspase-12-dependent apoptotic pathway in ionic radiocontrast urografin-induced renal tubular cell injury. *Toxicol. Appl. Pharmcol.* **266** (1), 167–175 (2013).
13. Jensen, S. J. K. Oxidative stress and free radicals. *J. Mol. Struct.* **666–667**, 387–392 (2003).
14. Sies, H. On the history of oxidative stress: Concept and some aspects of current development. *Curr. Opin. Toxicol.* **7**, 122–126. https://doi.org/10.1016/j.cotox.2018.01.002 (2018).
15. Zhao, Q. et al. Sulodexide protects contrast-induced nephropathy in sprague dawley rats. *Cell. Physiol. Biochem.* **40**, 621–632 (2016).
16. Kusirisin, P., Chattipakorn, S. C. & Chattipakorn, N. Contrast-induced nephropathy and oxidative stress: mechanistic insights. *J. Transl. Med.* **18** (1), 400. https://doi.org/10.1186/s12967-020-02574-8 (2020).
17. Myers, S. I., Wang, L., Liu, F. & Bartula, L. L. Iodinated contrast induced renal vasoconstriction is due in part to the downregulation of renal cortical and medullary nitric oxide synthesis. *J. Vasc. Surg.* **44**, 383–391 (2006).
18. Zhao, K., Gao, Q., Zong, C. & Li, Y. Combined anisodamine and probucol prevents contrast-induced nephropathy in diabetic rats by inhibiting p38 MAPK and Akt/mTOR/P70S6K signaling pathways. *Int. J. Clin. Exp. Med.* **12** (4), 3250–3260 (2019).
19. Owen, R. W. et al. The antioxidant/anticancer potential of phenolic compounds isolated from olive oil. *Eur. J. Cancer* **36**(10), 1235–1247. https://doi.org/10.1016/S0959-8049(00)00103-9 (2000).
20. Silva, S., Gomes, L., Leitao, F., Coelho, A. V. & Boas, L. V. Phenolic compounds and antioxidant activity of *Olea europaea* L. fruits and leaves. *Food Sci. Technol. Int.* **12**(5), 385–395. https://doi.org/10.1177/1082013206070166 (2006).
21. Visioli, F. & Galli, C. Biological properties of olive oil phytochemicals. *Crit. Rev. Food Sci. Nutr.* **42**(3), 209–221. https://doi.org/10.1080/10408690290825529 (2002).
22. Kwon, M. J. et al. The influence of tyrosol-enriched Rhodiola sachalinensis extracts bioconverted by the mycelium of bovista plumbe on scopolamine-induced cognitive, behavioral, and physiological responses in Mice. *Molecules* **27** (14), 4455 (2022).
23. Zargari, M. et al. Tyrosol and Olive oil ameliorate sodium arsenate-induced nephrotoxicity by modulating of oxidative stress and histological changes in mice. *Int. J. Prev. Med.* **14** (1), 47 (2023).
24. Karković Marković, A., Torić, J., Barbarić, M. & Jakobušić Brala, C. Hydroxytyrosol, tyrosol and derivatives and their potential effects on human health. *Molecules* **24** (10), 2001 (2019).
25. Shen, N. & Mao, X. Tyrosol and hydroxytyrosol: Current insights into biosynthesis, nutraceutical versatility, and human health. *Food Chemistry Advances* **1**, 101297 (2026).
26. Mateos, R., Sarria, B. & Bravo, L. Nutritional and other health properties of olive pomace oil. *Crit. Rev. Food Sci. Nutr.* **60** (20), 3506–3521 (2020).
27. Guo, J. et al. Inhibition of the NF-κB/HIF-1α signaling pathway in colorectal cancer by tyrosol: A gut microbiota-derived metabolite. *J. Immunother. Cancer* **12**(9), e008831 (2024).
28. You, L., Zhao, W., Li, X., Yang, C. & Guo, P. Tyrosol protects RPE cells from H_2O_2-induced oxidative damage in vitro and in vivo through activation of the Nrf2/HO-1 pathway. *Eur. J. Pharmacol.* **991**, 177316 (2025).
29. Kushwaha, R. et al. Bioactive compounds in the modulation of oxidative stress in monocytes and macrophages. *Sci. Rep.* **15**(1), 32012. (2025).

30. Wang, P. et al. Tyrosol attenuates ischemia–reperfusion-induced kidney injury via inhibition of inducible nitric oxide synthase. *J. Agric. Food Chem.* **61** (15), 3669–3675 (2013).
31. Yadav, T. C. et al. Exploration of interaction mechanism of tyrosol as a potent anti-inflammatory agent. *J. Biomol. Struct. Dyn.* **38**(2), 382–397 (2020).
32. Sendeski, M. M. Pathophysiology of renal tissue damage by iodinated contrast media. *Clin. Exp. Pharmacol. Physiol.* **38** (5), 292–299. https://doi.org/10.1111/j.1440-1681.2011.05503.x (2011).
33. Tveden-Nyborg, P., Bergmann, T. K., Jessen, N., Simonsen, U. & Lykkesfeldt, J. BCPT 2026 policy for experimental and clinical studies. *Basic Clin. Pharmacol. Toxicol.* **137**(6), e70159 (2025).
34. Çömez, M. et al. The effect of tyrosol on diclofenac sodium-induced acute nephrotoxicity in rats. *J. Biochem. Mol. Toxicol.* **38**(1), e23582 (2024).
35. Placer, Z. A., Cushman, L. L. & Johnson, B. C. Estimation of product of lipid peroxidation (malonyl dialdehyde) in biochemical systems. *Anal. Biochem.* **16** (2), 359–364 (1966).
36. Sedlak, J. & Lindsay, R. H. Estimation of total, protein-bound, and nonprotein sulfhydryl groups in tissue with Ellman's reagent. *Anal. Biochem.* **25**, 192–205 (1968).
37. Lawrence, R. A. & Burk, R. F. Glutathione peroxidase activity in selenium-deficient rat liver. *Biochem. Biophys. Res. Commun.* **71** (4), 952–958 (1976).
38. Aebi, H. I. Methods of enzymatic analysis. *Catalase* **1**, 673–686 (1983).
39. Kurien, B. T. & Scofield, R. H. Western blotting: an introduction. In *Western Blotting: Methods Protocols* 17–30. https://doi.org/10.1007/978-1-4939-2694-7_5 (2015).
40. Jiang, Y., Liu, Q., Zhao, Y., Wang, C. & Sun, M. Activation of CREB-BDNF pathway in pyramidal neurons in the hippocampus improves the neurological outcome of mice with ischemic stroke. *Mol. Neurobiol.* **60**(4), 1766–1781. https://doi.org/10.1007/s12035-022-03174-x (2023).
41. Güvenç, M. et al. Nobiletin attenuates acetaminophen-induced hepatorenal toxicity in rats. *J. Biochem. Mol. Toxicol.* **34**(2), e22427. https://doi.org/10.1002/jbt.22427 (2020).
42. Özkan, H., Kutlu, T., Yakin, A. & Özsoy, Ş. Y. Molecular, biochemical and histopathological effects of long term low and high percentage fructose consumption. *Ankara Üniversitesi Veteriner Fakültesi Dergisi*. **69** (4), 409–417 (2022).
43. Detrenis, S., Meschi, M., Musini, S. & Savazzi, G. Lights and shadows on the pathogenesis of contrast-induced nephropathy. *Br. J. Radiol.* **78** (936), 1064–1073. https://doi.org/10.1259/bjr/35368257 (2005).
44. Mehran, R. & Nikolsky, E. Contrast-induced nephropathy: definition, epidemiology, and patients at risk. *Kidney Int. Supplements*. **100**, S11–S15. https://doi.org/10.1111/j.1523-1755.2006.00273.x (2006).
45. Saha, S., Buttari, B., Panieri, E., Profumo, E. & Saso, L. An overview of Nrf2 signaling pathway and its role in inflammation. *Molecules* **25**(22), 5474. https://doi.org/10.3390/molecules25225474 (2020).
46. Wang, W. et al. Tyrosol effectively improves spermatogenesis recovery by S100A9/TLR4/NF-κB pathway in busulfan-induced oligozoospermia mice. *PeerJ* **14**, e20887. https://doi.org/10.7717/peerj.20887 (2026).
47. Ferlisi, F. et al. Olive mill waste-water extract enriched in hydroxytyrosol and tyrosol modulates host–pathogen interaction in IPEC-J2 cells. *Animals* **14**(4), 564. https://doi.org/10.3390/ani14040564 (2024).
48. Loboda, A., Damulewicz, M., Pyza, E., Jozkowicz, A. & Dulak, J. Role of Nrf2/HO-1 system in development, oxidative stress response and diseases: an evolutionarily conserved mechanism. *Cell. Mol. Life Sci.* **73** (17), 3221–3247. https://doi.org/10.1007/s00018-016-2223-0 (2016).
49. Wijerathne, C. U., Au-Yeung, K. K., Siow, Y. L. & O, K. 5-methyltetrahydrofolate attenuates oxidative stress and improves kidney function in acute kidney injury through activation of Nrf2 and antioxidant defense. *Antioxidants* **11**(6), 1046. https://doi.org/10.3390/antiox11061046 (2022).
50. Emad, M., El-Sherif, A. B. M., Abd-El Wahed, M. K. & Ahmed, R. M. Effect of urografin on the kidney of adult female albino rat and the possible protective role of nebivolol: A morphological and ultrastructural study. *Life Sci. J.* **10** (4), 248–261 (2013).
51. Toprak, O. et al. Preventive effect of nebivolol on contrast-induced nephropathy in rats. *Nephrol. Dialysis Transplant*. **23** (3), 853–859. https://doi.org/10.1093/ndt/gfm681 (2008).
52. Özbek, K. et al. The protective effect of single dose tadalafil in contrast-induced nephropathy: An experimental study. *Anatol. J. Cardiol.* **15**, 306–310. https://doi.org/10.5152/akd.2014.5380 (2015).
53. Kaspar, J. W., Niture, S. K. & Jaiswal, A. K. Nrf2:INrf2 (Keap1) signaling in oxidative stress. *Free Radic. Biol. Med.* **47**(9), 1304–1309. https://doi.org/10.1016/j.freeradbiomed.2009.07.035 (2009).
54. Lee, J. M. et al. Nrf2, a multi-organ protector?. *FASEB J.* **19**(9), 1061–1066. https://doi.org/10.1096/fj.04-2591hyp (2005).
55. Surh, Y. J., Kundu, J. K. & Na, H. K. Nrf2 as a master redox switch in turning on the cellular signaling involved in the induction of cytoprotective genes by some chemopreventive phytochemicals. *Planta Med.* **74**(13), 1526–1539. https://doi.org/10.1055/s-0028-1088302 (2008).

Publisher's note Springer Nature remains neutral with regard to jurisdictional claims in published maps and institutional affiliations.

Authors and Affiliations

Muhammed Etyemez[1] · Tuncer Kutlu[2]

✉ Muhammed Etyemez
muhammedetyemez@kastamonu.edu.tr

[1] Department of Physiology, Faculty of Veterinary, Kastamonu University, Kastamonu 37150, Turkey

[2] Department of Pathology, Faculty of Veterinary, Hatay Mustafa Kemal University, Hatay 31300, Turkey